General Disclaimer

One or more of the Following Statements may affect this Document

- This document has been reproduced from the best copy furnished by the organizational source. It is being released in the interest of making available as much information as possible.

- This document may contain data, which exceeds the sheet parameters. It was furnished in this condition by the organizational source and is the best copy available.

- This document may contain tone-on-tone or color graphs, charts and/or pictures, which have been reproduced in black and white.

- This document is paginated as submitted by the original source.

- Portions of this document are not fully legible due to the historical nature of some of the material. However, it is the best reproduction available from the original submission.

NASA Contractor Report 168280

EFFECT OF CRACK CURVATURE ON STRESS INTENSITY FACTORS FOR ASTM STANDARD COMPACT TENSION SPECIMENS

Javed Alam and Alexander Mendelsen

Case Western Reserve University
Cleveland, Ohio

October 1983

Prepared for

NATIONAL AERONAUTICS AND SPACE ADMINISTRATION
Lewis Research Center
Under Grant NSG3-251

INTRODUCTION

The use of linear elastic fracture mechanics in the design of structures requires the knowledge of the fracture toughness of the material. For this purpose the ASTM has established a standard test method, (E399) for obtaining the plane-strain fracture toughness of a given material, [1]. One of the standard specimens used in such a test is the compact tension specimen (CTS) shown in figure 1.

Very rigid standards have been imposed in reference [1] to insure that valid fracture toughness values will be obtained in a given test. One of the requirements is the production of a fatigue crack. However, the fatigue crack will usually not grow uniformly across the specimen thickness, i.e. the initially straigth crack front will become curved. The crack length thus varies across the specimen thickness and some average value must be used to calculate the fracture toughness. A standard measure is provided in reference [1] such that if the crack front curvature, as measured after the specimen is broken, is greater than this standard measure, the test is invalid.

Recently, however, suggestions have been made, [2] that the above standard is too rigid and can be relaxed since the effect of the curved crack front may be less than originally anticipated. These suggestions, however, are based on rather weak evidence, [3] and it is not yet clear whether the E 399 standard should be relaxed or not in this respect. What is needed is a clear definitive analysis of the effect of the crack front curvature on the stress intensity factor. The objective of this investigation is to perform this analysis.

Several three-dimensional finite element analyses have been made of the compact tension specimen, e.g. [4,5]. These analyses showed that for the CTS, the stress intensity factor is a maximum at the center of the specimen and a

minimum at the surface of the specimen. When crack curvature is introduced, the maximum stress intensity factor moves to the surface of the specimen and the minimum occurs at the center. The dimensions of the specimens treated in these analyses differed from those of the standard specimen. A few attempts have also been made to determine experimentally the effect of crack tip curvature using a 3-D stress freezing technique [6], and scattered light speckle interferometry [7]. Both these investigations showed qualitative agreement with the above results.

The present investigation uses the method of lines (MOL) to obtain an accurate three-dimensional solution for the standard CTS with curved crack fronts. The MOL is described fully in references [8] and [9], where it is also shown that accurate solutions of crack problems can be obtained. An improved version of the method and the application to the standard CTS with a straight crack front has been presented in a previous paper, [10]. The method will be only briefly reviewed here for completeness.

BACKGROUND OF THE METHOD OF LINES

Within the framework of linearized elasticity theory, the equations of elastic equilibrium in terms of displacements are

$$G\,\nabla^2 u_i + (\lambda + G)\,\theta_{,i} = 0 \quad , i = 1, 2, 3 \tag{1}$$

$$\theta = u_{j,j}$$

where λ and G are Lame's constants, u_i are the displacement and the usual tensor notation is used.

For a finite geometry solid we construct three sets of parallel lines, Fig. 2. Each set of lines is parallel to one of the coordinate axes and thus perpendicular to the corresponding coordinate plane. An approximate solution

of Eq. (1) can then be obtained by developing solutions of ordinary differential equations along the x-directional lines. As seen in the figure, there are a total of $\ell = NY \times NZ$ such lines where NY is the number of lines along the y-direction and NZ is the number of lines along the z-direction in a given plane, respectively. We define the displacements along these lines as $u_1, u_2, \ldots u_\ell$. The derivatives of the y-directional displacements on these lines with respect to y are defined as $v'|_1, v'|_2, \ldots, v'|_\ell$, and the derivatives of the z-directional displacements with respect to z are defined as $w'|_1, w'|_2, \ldots, w'|_\ell$. These displacements and derivatives can then be regarded as functions of x only since they are variables on x-directional lines. When these definitions are used, the ordinary differential equation along a generic line ij using a 5-point difference formula, may be written as:

$$\frac{d^2u_{ij}}{dx^2} - \frac{(1-2\nu)}{2(1-\nu)}\left[\frac{1}{12h_y^2}\left(u_{i-2,j} - 16u_{i-1,j} + 30u_{ij} - 16u_{i+1,j} + u_{i+2,j}\right) + \frac{1}{12h_z^2}\left(u_{i,j-2} - 16u_{i,j-1} + 30u_{ij} - 16u_{i,j+1} + u_{i,j+2}\right)\right] + \frac{d}{dx}\frac{f_{ij}(x)}{2(1-\nu)} = 0 \qquad (2)$$

where

$$f_{ij}(x) = v' + w'; \; v' = \frac{dv}{dy} \text{ and } w' = \frac{dw}{dz} \qquad (3)$$

Similar differential equations are obtained along the other x-directional lines. Since each equation has the terms of the displacement on the surrounding lines, These equations constitute a system of ordinary differential equations for the displacements $u_1, u_2 \ldots, u_\ell$. It is to be noted that for lines lying on or near a boundary appropriate noncentral difference formulas must be used. Also, the shear boundary conditions are incorporated in these equations as described in reference [9].

The set of ℓ second order differential equations represented by Eq. (2) can be reduced to a set of 2ℓ first order differential equations by treating the derivatives of the u's as an additional set of ℓ unknowns.

$$u_{\ell+1} = \frac{du_1}{dx} \ , \ u_{\ell+2} = \frac{du_2}{dx} \ , \text{ etc.} \tag{4}$$

The resulting 2ℓ equations can now be written as a single first order matrix differential equation

$$\frac{dU}{dx} = A_1 U + \frac{dR(x)}{dx} \tag{5}$$

where U and R are column matrices of 2ℓ elements each and A_1 is a 2ℓ x 2ℓ matrix of the constant coefficients appearing in Eqs. (2) and (4).

In a similar manner, to solve Eq. (1) for i = 2 and 3 ordinary differential equations are constructed along the y- and z-directional lines, respectively. These equations are also expressed in an analogous form to Eq. (5); they are

$$\frac{dV}{dy} = A_2 V + \frac{dS(y)}{dy} \tag{6}$$

$$\frac{dW}{dz} = A_3 W + \frac{dT(z)}{dz} \tag{7}$$

Equations (5) to (7) are linear first-order ordinary matrix differential equations. They are, however, not independent, but are coupled through the vectors R, S, and T whose components are given by equations similar to Eq. (3). They must therefore be solved iteratively correcting R, S and T after each iteration. The elements of the coefficient matrices A_1 , A_2, and A_3 are all constants, being functions of the coordinate increments and Poisson's ratio only.

To solve equations (5) - (7) a recurrence relation algorithm was set up as described in detail in reference (10). This algorithm is particularly useful

for solving two-point boundary value problems, requiring one sweep through from one boundary to the opposite one to obtain the missing boundary conditions and a second sweep through to obtain the complete solution everywhere.

CALCULATION OF STRESS INTENSITY FACTOR

The stress intensity factor K_I is defined as follows:

$$K_I = \lim_{R \to 0} \sigma_y (2\pi R)^n$$

where R is measured from the crack tip and is normal to the crack front. n is the singularity. It was found, however, that due to the coarseness of the grid used, the usual plotting and extrapolating techniques gave results that were erratic and of questionable accuracy. This was compounded by the fact that the precise crack tip location is not really known except that it is approximately midway between two lines, one of which has zero stress specified. It was found, however, that by using two terms in the stress and displacement series expansions around the crack tip, good results could be obtained even with the coarse grid used. Furthermore, this also permitted the determination of the actual crack tip location from the computed results. The method utilized is as follows, [11], we take

$$v|_{y=0} = \alpha K_I \left[\sqrt{\frac{R + r}{2\pi}} + \frac{L_I}{K_I} \sqrt{(R + r)^3} \right] \quad . . \tag{8}$$

$$\sigma_{y|y=0} = K_I \left[\frac{1}{\sqrt{2\pi(R - r)}} + \frac{L_I}{K_I} \sqrt{(R - r)} \right] \tag{9}$$

where α is a function of Poisson's ratio, n was assumed to be $-\frac{1}{2}$, and r is the crack edge position correction measured from the originally assumed midpoint position. Using displacement data from three adjacent nodes to the crack edge

in Eq. (8), values of αK_I, L_I/K_I and r are calculated for each value of z, with R also measured from the halfway point between nodes specifying boundary stresses and displacements, respectively. Note that α would be equal to 3.56 for the plane strain case and 4.0 for the plane stress case. In the case of curved crack fronts a normal is drawn at the point where K_I is determined. The displacement values at the points where the normal meets the grid lines are extrapolated using the nodal displacement values. These extrapolated values of - placement are used to obtain the local K_I values for the curved crack fron

RESULTS AND DISCUSSION

The MOL was first applied to a compact tension specimen with tensile loading. The specimen dimensions were W/a = 2.0, B/a = 1.0 and L/a = 2.4. Where a, B, W and L are the crack length, specimen thickness, width and length respectively. Crack length to width ratio was maintained close to 0.5. Figures 2 and 3 show the coordinate system and line number designation.

Figure 4 shows a plot of the local stress intensity factor variation through the thickness of the specimen with tensile loading. Curve 1 is for a straight crack front. For this case the maximum SIF occurs at the center of the specimen. It drops by 13 percent on the surface. This trend is in accordance with the previously reported results of Raju (12).

The remaining curves in the figure are for increasing crack tunnel depth. Crack tunnel depth is defined as the difference between the crack lengths at the center and the surface of the specimen. Since approximate parabolic curves were used in the study, it was difficult to assign a single crack curvature for the crack front. An increasing crack tunnel depth reflects an increasing crack curvature. For crack tunnel depth of 0.1 we see that SIF decreases at the center by 9.5 percent, while at the surface its value increases by 20.5 percent. Similar type of variation is reported by Pereira [4]. However, a direct comparison of

the results is not possible because a different crack and specimen size were used in that study. Herein, the dimensions prescribed in ASTM standard [1] are used.

For higher crack tunnel depths the maximum SIF value no longer occurs at the surface, but shifts to the adjacent interior point of the grid. This trend is not reported in reference [4]. There could be two possible reasons for this differece, 1) the crack length a/W used in reference [4] is 0.25 which is smaller than the one used in the present study, 2) three layers of elements were taken in the thickness direction, possibly causing the maximum SIF to be missed.

Figure 5 shows the variation of the non-dimensional SIF for the same specimen with a parabolic shear load along the load line. The results are similar to those of figure 4 for the tensile loading.

Figure 6 shows the variation of center (C), surface (S) and thickness average (av) stress intensity factors with increasing crack tunnel depth for a standard compact tension specimen under shear loading. The stress intensity factors are non-dimensionalized with the respective values of SIF occuring for a straight crack front (SC). We find that non-dimensional SIF value at the center of the specimen keeps on decreasing as the crack tunnel depth increases. However, the value of SIF at the surface increases to a maximum and then decreases. The thickness average SIF constantly decreases with increasing crack tunnel depth. Similar trend for the thickness average SIF was observed by McGowan [6] in his study on single edge notch specimen. This figure shows clearly that the presence of a curved crack front can significantly change the value of the stress intensity factor.

In figure 7 the change in the thickness average SIF is plotted with a non-dimensional factor η. The value of η corresponds to the difference between the average crack length (a_{av}) and the surface trace of the crack divided by the

average crack length (a_{av}). The calculation of a_{av} is done by computing an average of the three crack measurements taken at the center of the crack front and midway between the center and the end of the crack front on each side, which is the definition used in [1]. Reference [1] restricts the length of either surface trace of the crack to greater than 90 percent of the average crack length (a_{av}). Based on this criterion, the ASTM region is marked on the figure 7. Any test in which the specimen has a surface trace within the marked region is considered a valid test. For the worst case when the surface trace is 90 percent of a_{av} in the specimen, there is a 7 percent lowering in the thickness average stress intensity factor, which indicates that the use of plane strain formula given in reference [1] will result in an overestimation of the fracture toughness of a material by 7 percent.

On the basis of the experimental results and three-dimensional analysis of Neale and Pereira [4,5], an amendment has recently been incorporated, [13] to extend the limit on the surface trace to 85 percent of average crack length. This figure corresponds to a η value of 15 percent. From the figure 7 we find a lowering of 12.5 percent in the thickness average SIF for this value of η. This implies that the use of two-dimensional plane strain formula will result in an overestimation of the fracture toughness of a material by 12.5 percent. These figures thus show the effect of crack curvature on the overestimation of the fracture toughness for the compact tension specimen.

CONCLUSIONS AND RECOMMENDATIONS

1) The results from the numerical analysis show that the stress intensity factor decreases at the center of the compact specimen due to crack curvature. For the low values of crack tunnel depth the maximum stress intensity factor is found to be at the surface of the specimen. If the crack tunnel depth is

increased, the maximum value of stress intensity factor no longer remains at the surface, but shifts to an interior point of the specimen, still remaining close to the surface.

2) The average value of stress intensity factor through the thickness keeps on decreasing with increasing crack tunnel depth.

3) The ASTM test method [1] allows either surface trace of the crack to be less than 90 percent of the average crack length. Based on an average SIF calculation, this will overestimate the fracture toughness by 7 percent. It is further estimated that the new amendment changing the 90 percent to 85 percent will lead to an overestimation of fracture toughness by 12.5 percent.

The plots for stress intensity factor through the thickness of compact tension specimen for two different types of loading predict that the crack growth should start at the surface of the specimen first. This conclusion from analytical study is contrary to the experimentally observed crack propagation. It is anticipated that plastic flow can significantly change the stress conditions existing at the surface, which is, of course, not accounted for in an elastic analysis. Neale [14] developed an elasto-plastic model to fix this discrepancy, but it is an approximate analysis. To fully study the problem, we need to analyze a full three-dimensional elastic-plastic case. The results of such a study will be presented in a subsequent publication.

REFERENCES

1. Standard Test Method for Plane-Strain Fracture Toughness of Metallic Materials, ANSI/ASTM E399-78.

2. Private communication from J.G. Kaufman, Chairman of ASTM Committee E-24 on Fracture Testing to W.F. Brown, Jr., NASA Lewis Research Center, Cleveland, Ohio.

3. Private Communication from W.F. Brown, Jr., to J.G. Kaufmann.

4. Pereira, M.F.S., Head, J.L. and Turner, C.E., "Three Dimensional Crack Analysis Using Standard Isoparametric Elements", Report of the Imperial College of Science and Technology, London.

5. Neale, B.K., "The Influence of Crack Shape on Fracture Toughness Testing", Int. J. of Fracture, Vol. 12 (1976), p. 499-502.

6. McGowan, J.J., "A Photoelastic Investigation of the Effect of Crack Front Curvature on the Stress Intensity Factor Distribution in a Single Edge Notch Specimen", BER 242-97, September, 1977.

7. Fourney, M.E., "Experimental Determination of the Effect of Crack Front Curvature in an ASTM Compact Tension Specimen", Proceedings of the Fourth Brazilian Congress of Mechanical Engineering, 1977, p. 13-26.

8. Gyekeneyai, J.P., "Solution of Some Mixed Boundary Value Problems of Three-Dimensional Elasticity by The Method of Lines", Ph.D. Thesis, Michigan State University, 1972.

9. Gyekenyesi, J.P. and Mendelson, A., "Three Dimensional Elastic Stress Analysis of Finite Geometry Solids Containing Cracks", Int. J. of Fracture, Vol. 11, No. 3, June, 1975.

10. Mendelson, A. and Alam, J., "The Use of the Method of Lines in 3-D Fracture Mechanics Analysis with Applications to Compact Tension Specimens", Submitted to Int. J. of Fracture.

11. Gyekenyesi, J.P. and Mendelson, A., "Stress Analysis and Stress Intensity Factors for Finite Geometry Solids Containing Rectangular Surface Cracks", J. of Appl. Mech., Trans. ASME, Vol. 44, Series E, No. 3, Sept. 1977.

12. Raju, I.S. and Newman, J.C., Jr., "Three-Dimensional Finite Element Analysis of Finite-Thickness Fracture Specimens", NASA TND-8414, 1977.

13. Standard Test Method for Plane-Strain Fracture Toughness of Metallic Materials, ASTM E399-81.

14. Neale, B.K., "The Stress Intensity Factors Associated with Curved Crack Fronts in a Compact Tension Specimen", Proc. of the First International Conference on Numerical Methods in Fracture Mechanics, Swansea, 1978, Ed. A.R. Luxmoore and D.R.J. Owen, p. 218-224.

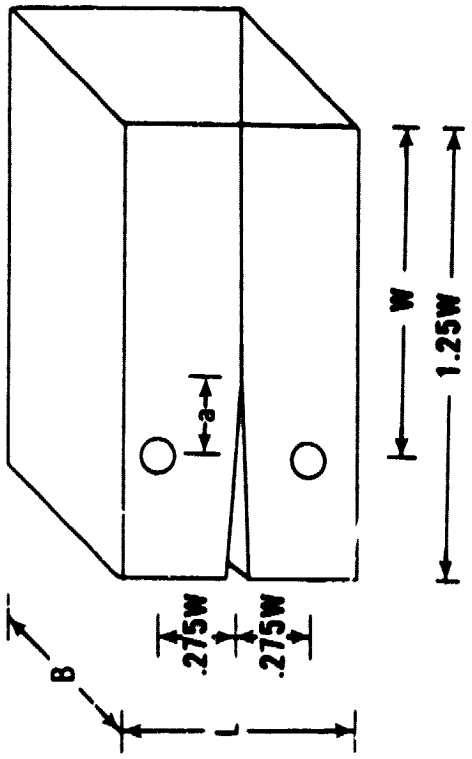

Figure 1. Compact tension specimen.

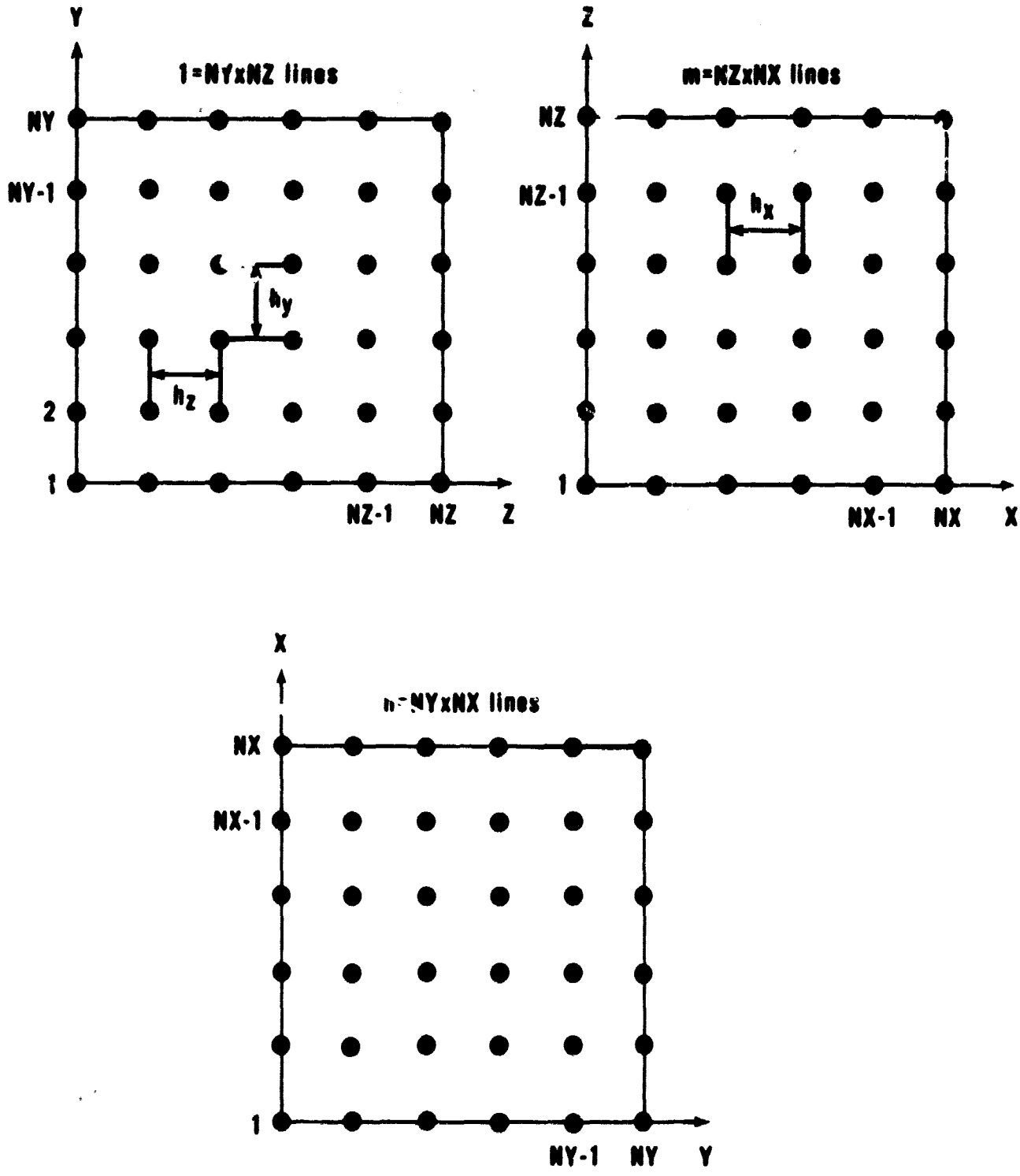

Figure 2. Three sets of lines parallel to X-, Y-, and Z-coordinates and perpendicular to corresponding coordinate planes.

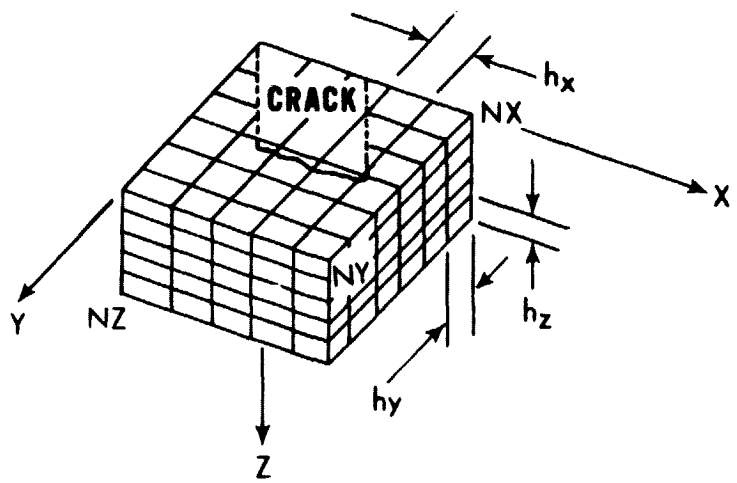

Figure 3. Coordinate system and line numbering for single edge notch and compact tension specimens.

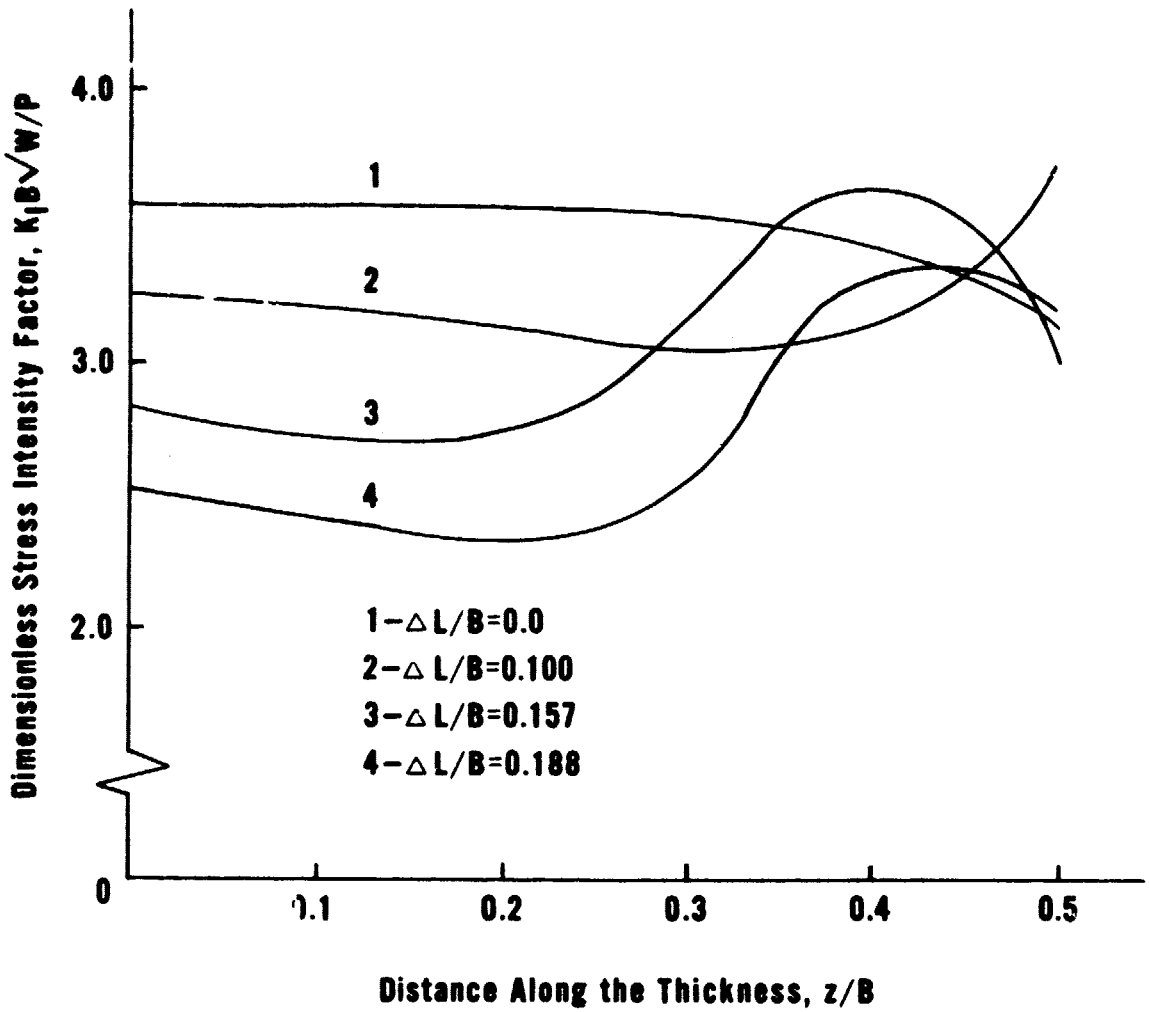

Figure.4. Variation of dimensionless SIF with thickness for different crack tunnel depths for compact tension specimen under tensile loading.

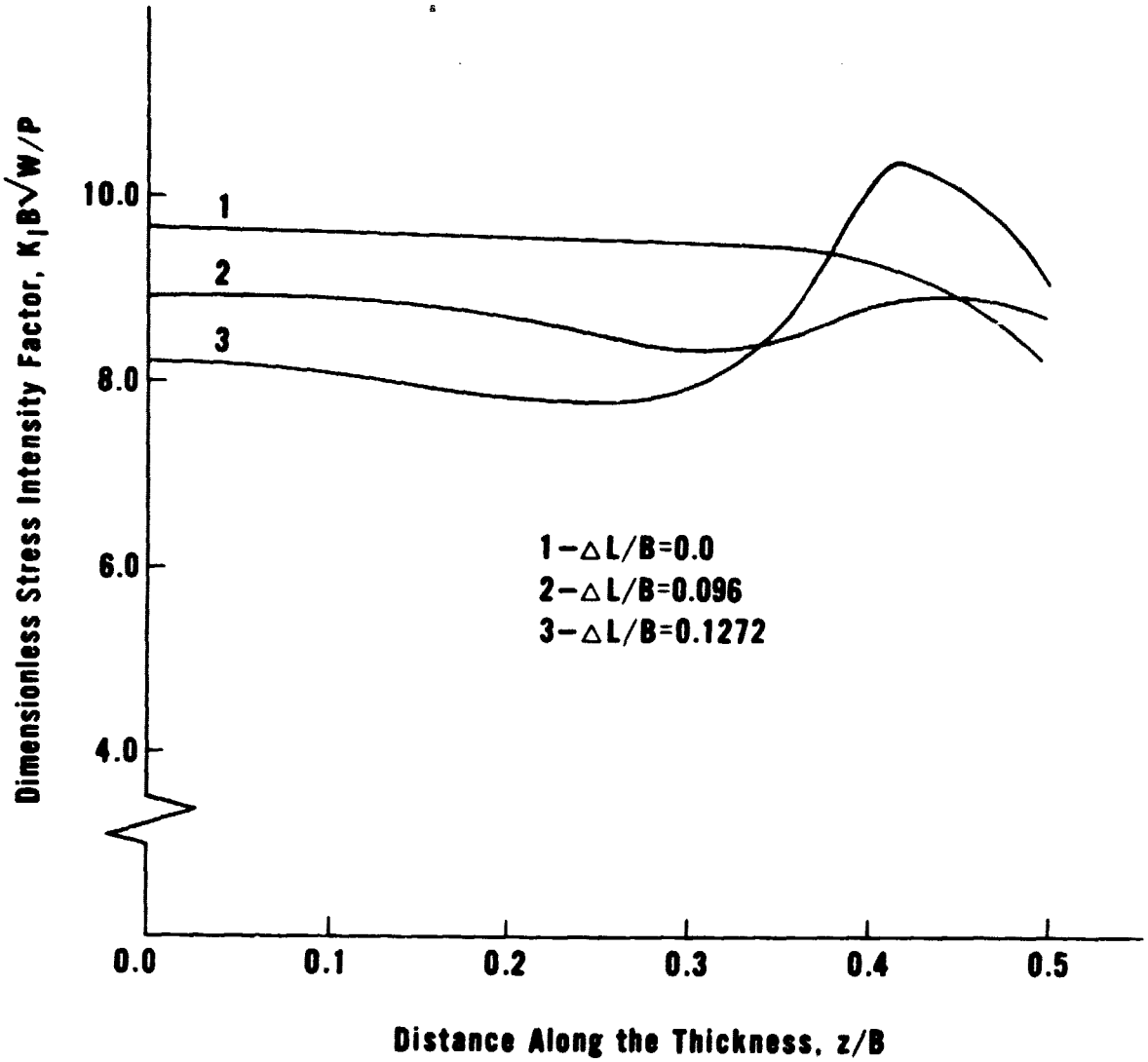

Figure 5. Variation of dimensionless SIF through the thickness for different crack tunnel depths, for compact tension specimen under parabolically applied shear load.

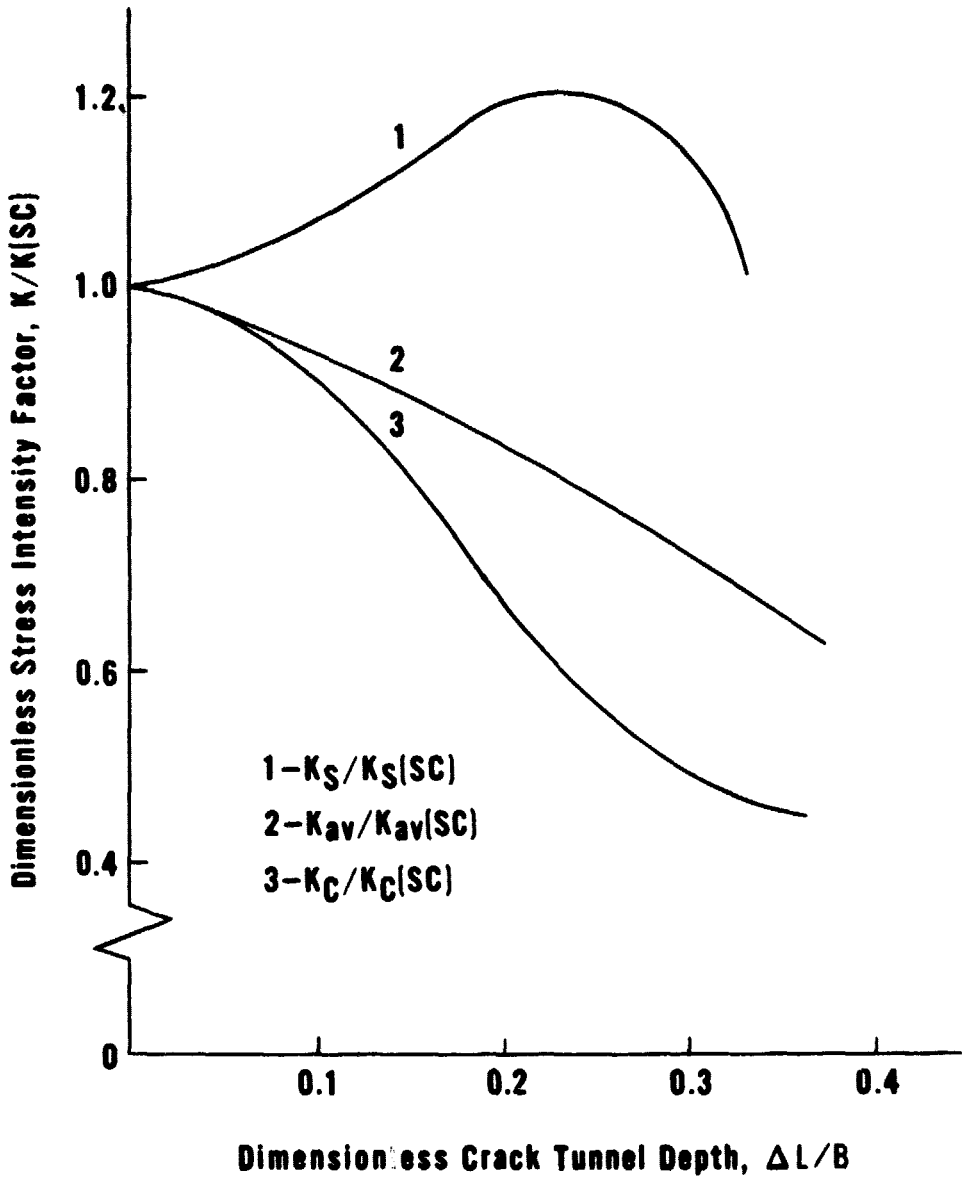

Figure 6. Variation of center, surface and thickness average stress intensity factor with increasing crack tunnel depth.

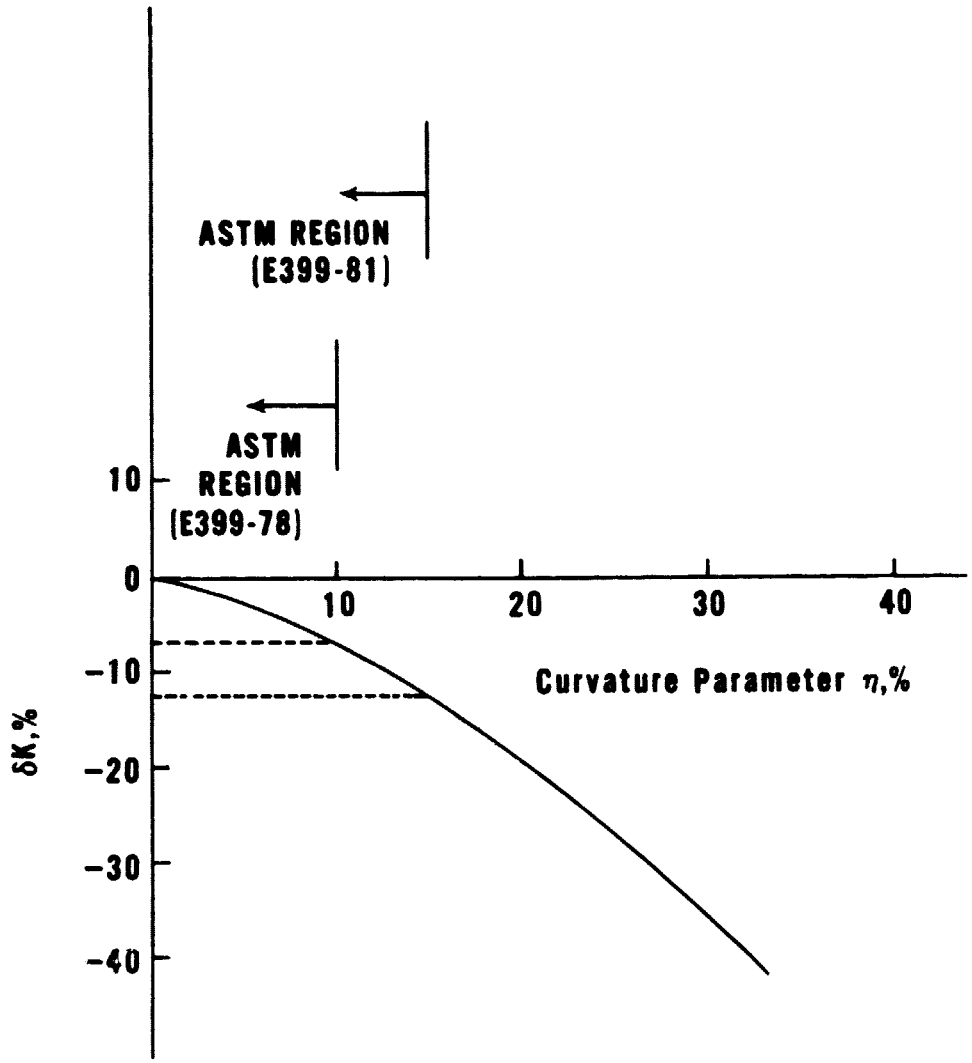

Figure 7. Percent variation in average stress intensity factors between straight crack and curved crack fronts.